Title	Correlation between Am(III)/Eu(III) selectivity and covalency in metal-chalcogen bonds using density functional calculations
Author(s)	Kaneko Masashi, Watanabe Masayuki
Citation	Journal of Radioanalytical and Nuclear Chemistry, 316(3),p.1129-1137
Text Version	Accepted Manuscript
URL	https://jopss.jaea.go.jp/search/servlet/search?5058955
DOI	https://doi.org/10.1007/s10967-017-5683-2
Right	This is a post-peer-review, pre-copyedit version of an article published in Journal of Radioanalytical and Nuclear Chemistry. The final authenticated version is available online at: https://doi.org/10.1007/s10967-017-5683-2

Correlation between Am(III)/Eu(III) selectivity and covalency in metal-chalcogen bonds using density functional calculations

Masashi Kaneko*, Masayuki Watanabe

Nuclear Science and Engineering Center, Japan Atomic Energy Agency, 2-4, Shirakata, Tokaimura, Ibaraki, 319-1195, Japan

Abstract

We applied density functional theory calculations to Am(III) and Eu(III) complexes with chalcogen-donor ligands of the formula $N(EPMe_2)_2^-$ (E = O, S, Se, Te). We calculated the equilibrium structures and relative stabilities of the complexes in the complexation reaction. The results indicated that the tendency of the relative stability is O << S ~ Se ~ Te, which is consistent with the trend of soft acid classification. Molecular orbital overlap population analysis suggested that this tendency can be correlated with the bonding type in the covalent interaction between the f-orbitals of the metal atom and the chalcogen-donor atoms.

Keywords

partitioning and transmutation, minor-actinides separation, f-block chemistry, density functional calculation, chemical bonding, hard and soft acids and bases

Introduction

Minor-actinides (MA = Np, Am, Cm), which have extremely long half-lives and high radiotoxicity, are presented in high-level radioactive liquid waste generated during the

22   reprocessing of spent nuclear fuels. The selective separation of MA from lanthanides

23   (Ln) is required to carry out one rational disposal method, in which MA are separated

24   from high-level radioactive waste followed by the transmutation of MA (*i.e.*, the

25   partitioning and transmutation strategy), because Ln have a high reaction cross-section to

26   neutrons and inhibit the transmutation of MA [1]. However, the similarity of the chemical

27   properties (*e.g.*, stability, chemical reactivity, and coordination geometry) between

28   trivalent MA(III) (Am(III), Cm(III)) and Ln(III) ions hinders the selective separation of

29   MA(III) ions from Ln(III) ions [2].

30   Solvent extraction has been employed as a powerful tool to separate MA(III) ions from

31   Ln(III) ions, which has demonstrated the dependence of the selectivity on the donor

32   atoms of the extraction reagents. For example, O-donor reagent such as dialkylphosphinic

33   acids (HO_2PR_2) selectively separate Ln(III) ions over MA(III) ions, whereas S-donor

34   reagents such as dialkyldithiophosphinic acids (HS_2PR_2) selectively separate MA(III)

35   ions over Ln(III) ions [3]. The tendency of this selectivity can be explained by reference

36   to the hard and soft acids and bases (HSAB) rule [4]. When comparing the stabilities of

37   complexes with chalcogen-donor ligands, hard metal ions form more stable complexes

38   with O-donor ligands than S, Se, and Te-donor ligands, whereas soft metal ions form

39   more stable complexes with S, Se, and Te-donor ligands than O-donor ligands [4]. If it is

40   assumed that Ln(III) ions are harder than MA(III) ions or MA(III) ions are softer than

41   Ln(III) ions, we can understand the difference in MA(III)/Ln(III) selectivity between O-

42   donor and S-donor reagents. This assumption is based on computational results using

43   relativistic quantum chemical calculations on MA(III) and Ln(III) ions, which concluded

44   that the radial distribution of valence d- and f-orbital electrons in MA(III) ions is larger

45   than that in Ln(III) ions [5]. This should cause MA(III) ions to exhibit soft character

46   owing to the stronger covalent interactions between MA(III) ions and ligands. It is,

47   however, still unclear whether the valence orbitals of MA(III) ions participate in

48   coordination bonds in the formation of complexes.

49   Density functional theory (DFT) has been employed as a powerful tool to understand the

50   chemical bonding, stability, and reactivity of f-block complexes [6-9]. Recently, it has

51   been used to study the separation of Am(III) ions from Eu(III) ions using HO_2PR_2 and

52 HS_2PR_2 ligands as S-donor and O-donor extraction reagents, respectively [10, 11]. Our

53 previous work has indicated that DFT method using double hybrid exchange-correlation

54 functional, B2PLYP, reproduced the Am(III)/Eu(III) selectivity of S-donor and O-donor

55 reagents by comparing their relative stability in the complexation reaction [12]. We also

56 suggested that the contribution of valence f-orbital electrons in Am(III) ions to

57 coordination bonds, rather than the contribution of the d-orbitals, is critical to the relative

58 stability in Am(III) complexes in comparison with Eu(III) complexes, which leads to a

59 difference in Am(III)/Eu(III) selectivity between S- and O-donor reagents [13]. However,

60 it has not yet been decided whether the selectivity is entirely due to the contribution of f-

61 orbitals, which is because differences in coordination geometry and symmetry between

62 the S-donor complex, $[M(S_2PR_2)_3]$ (Figure 1a), in which three equivalents of the

63 monomeric HS_2PR_2 ligand coordinate to one metal ion, and the O-donor complex,

64 $[M\{(O_2PR_2)_2H\}_3]$ (Figure 1b), in which three equivalents of dimeric HO_2PR_2 coordinate

65 to one metal ion, may contribute to the occurrence of selectivity.

66 In this paper, we focus on the Am(III)/Eu(III) selectivity of chalcogen-donor reagents

67 that   form   complexes   with   the   same   coordination   mode.   The

68 bis(chalcogenophosphinyl)imine ligands $HN(EPR_2)_2$ (E = O, S, Se, and Te) can bond to

69 trivalent f-block metal ions with the same coordination symmetry irrespective of

70 differences of the chalcogen-donor atom (Figure 1c), which enables us to investigate the

71 systematic trends in the covalency of the metal-chalcogen bonds [14, 15]. The present

72 study aimed to correlate the Am(III)/Eu(III) selectivity with the bonding contribution of

73 the valence orbitals of the metal ions to their covalent interaction with the chalcogen-

74 donor atoms. We modeled the complexes of Eu(III) and Am(III) ions with $HN(EPR_2)_2$

75 ligands with reference to analogous crystal structures [14, 15] and predicted the

76 Am(III)/Eu(III) selectivity of the chalcogen-donor ligands using a previously reported

77 procedure [12]. Finally, we discuss the correlation of the selectivity with the covalency of

78 the metal-chalcogen bonds by electron population analyses of the valence orbitals of the

79 metal ions in their complexes. We expect that this study will provide guidelines for the

80 design of novel extraction reagents for the separation of MA(III) ions from Ln(III) ions

81 because there have thus far been no relevant investigations, which mention that the

82 separation of MA(III) ions might be improved by strengthening the chemical bonding

83 between the metal ions and the extraction reagents.

84 **Computational details**

85 Model complexes of the formula $[M\{N(EPMe_2)_2\}_3]$ (M = Eu, Am; E = O, S, Se, Te),

86 were created with reference to single crystal X-ray structures, namely, $[Eu\{N(OPPh_2)_2\}_3]$

87 [15], $[La\{N(SP^iPr_2)_2\}_3]$ [14], $[La\{N(SeP^iPr_2)_2\}_3]$ [14], $[Ce\{N(TeP^iPr_2)_2\}_3]$ [14]. Starting

88 coordinates for geometry optimization calculations were set by replacing the phenyl or

89 isopropyl groups of the phosphine moieties by methyl groups. We note that in general

90 Am(III) complexes have the same crystal system and similar coordination geometries to

91 Ln(III) complexes, as reported in several papers [16-18]. In this paper, we focus on the

92 structure, stability, and bonding properties of only the Δ conformer of the

93 $[M\{N(EPMe_2)_2\}_3]$ complex, because our previous studies indicated that differences

94 between conformers have only minor effects on the equilibrium structure and relative

95 stability in complexation reactions [13, 19]. The model of the complexation reaction is

96 described by Eq. 1 and the difference in Gibbs energy (ΔG) in the reactions was

97 estimated by Eq. 2:

98 $[M(H_2O)_9]^{3+} + 3\,N(EPMe_2)_2^- \rightarrow [M\{N(EPMe_2)_2\}_3] + 9\,H_2O$ (1)

99 $\Delta G = [G([M\{N(EPMe_2)_2\}_3]) + 9\,G(H_2O)] - [G([M(H_2O)_9]^{3+}) + 3\,G(NEPMe_2^-)]$ (2)

100 The Gibbs energy (G) can be divided into the total energy (E^{tot}) and a thermal correction

101 term for Gibbs free energy (G^{corr}), which were obtained by single-point energy

102 calculations and calculations on normal frequency modes, respectively (Eq. 3). The G^{corr}

103 term includes a thermal correction for an enthalpy term (H^{corr}), an entropy term (S), and

104 the temperature (T), as shown in Eq. 4. The H^{corr} term is defined as the sum of the

105 vibrational energy (E^{vib}), rotational energy (E^{rot}), translational energy (E^{trans}), and k_BT,

106 where k_B denotes the Boltzmann constant (Eq. 5). The S term is defined as the sum of the

107 spin entropy (S^{spin}), vibrational entropy (S^{vib}), rotational entropy (S^{rot}), and translational

108 entropy (S^{trans}), as shown in Eq. 6:

109    $G = E^{\text{tot}} + G^{\text{corr}}$ (3)

110    $G^{\text{corr}} = H^{\text{corr}} - TS$ (4)

111    $H^{\text{corr}} = E^{\text{vib}} + E^{\text{rot}} + E^{\text{trans}} + k_{\text{B}}T$ (5)

112    $S = S^{\text{spin}} + S^{\text{vib}} + S^{\text{rot}} + S^{\text{trans}}$ (6)

113   The E^{rot} and S^{rot} terms were calculated under the rigid-rotator approximation with the

114   assumption that the symmetric number for all the metal complexes is 3. The E^{vib} and S^{vib}

115   terms were calculated under the quasi-harmonic approximation, which is the same as the

116   usual harmonic oscillator approximation, except that vibrational frequencies less than 60

117   cm^{-1} were increased to 60 cm^{-1} to correct for the well-known beakdown of the harmonic

118   oscillator model for the free energies of low-frequency vibrational modes [20, 21].

119   All DFT calculations were performed using ORCA ver. 3.0 package [22]. A zeroth-order

120   regular approximation (ZORA) Hamiltonian compensated by perturbative spin-orbit

121   coupling effects was employed to consider all-electron scalar relativistic effects [23, 24].

122   Geometry optimization and single-point energy calculations were performed using the

123   BP86 functional [25, 26] in the gas phase and the B2PLYP functional [27] in the aqueous

124   phase, respectively, of which the performance was confirmed in our previous works [28].

125   In both sets of calculations, segmented all-electron relativistically contracted (SARC)

126   basis sets, which were optimized for ZORA calculation, were assigned to all atoms [29-

127   31]. The SVP for geometry optimization and the TZVP for single-point energy

128   calculations were assigned to non-metal atoms. The spin multiplet of the electronic

129   ground state for the Eu(III) and Am(III) complexes was set to the spin septet state. The

130   unrestricted Kohn-Sham method was employed for open-shell systems. The solvation

131   effect of water was considered using a conductor-like screening model (COSMO) method

132   for single-point energy calculations, in which the COSMO radii for Eu(III) and Am(III)

133   ions were set to 1.99 and 1.90 Å, respectively [32, 33]. Resolution of the identity

134   approximations employed the Split-RI-J method [34] for pure DFT calculations and the

135   RIJCOSX method [35] for hybrid DFT calculations in order to reduce the computing cost

136   for two-electron integral terms in self-consistent field (SCF) calculations. The

137   convergence threshold and grid resolution for SCF iterations were set to the same

138   conditions as in our previous work [12]. Three-dimensional descriptions of optimized

139   structures and molecular orbitals (MOs) were visualized using the VESTA program [36].

140   Analyses of spin populations and MO overlap populations (MOOPs) using Mulliken's

141   methods [37, 38] were performed to discuss the properties of the bonding between the

142   metal ion and the chalcogen-donor atoms in $[M\{N(EPMe_2)_2\}_3]$.

143   **Results and discussions**

144   *Geometry optimization*

145   All the equilibrium geometries of the metal complexes were obtained as local minimum

146   structures, which were confirmed by calculations of vibrational frequency modes. Table 1

147   shows the metal-chalcogen distances for $[M\{N(EPMe_2)_2\}_3]$. The average Am-E bond

148   lengths were shorter than the average Eu-E bond lengths except for $[M\{N(OPMe_2)_2\}_3]$.

149   This tendency, as well as the absolute values of the M-E distances, is consistent with

150   previously reported results of calculations for $[M\{N(EPH_2)_2\}_3]$ (M = Eu, Am; E = O, S,

151   Se, Te) [39], as shown in Table 1. These calculated values could reproduce experimental

152   bond lengths determined for analogous complexes that possess La(III) or Pu(III) as the

153   central metal. This indicates that the replacement of $-P^iPr_2$ or $-PPh_2$ groups by $-PMe_2$ or -

154   PH_2 groups in the $N(EPR_2)_2$ ligand has only a minor effect on predictions of the

155   equilibrium structures of the complexes by geometry optimization. We also found that

156   the nature of the bonding is essentially ionic, because the bond lengths almost correspond

157   to the sum of the Shannon's effective ionic radii (r^{ion}) of M^{3+} and E^{2-} [40], as shown in

158   Table 1. The coordination geometries of $[M\{N(EPMe_2)_2\}_3]$ are compared in Figure 2 and

159   are shown to belong to the pseudo-D_3 point group, in which a C_3 rotational axis extends

160   perpendicular to the plane that includes the three nitrogen atoms through the central metal

161   atom and three sets of C'_2 axes intersect the lines that join the central metal atom and the

162   nitrogen atoms, independently of the metal atom or chalcogen atoms. The averaged E-M-

163   E bond angles were 82.7(2)°/81.7(1)°, 87.9(14)°/87.6(1)°, 90.2(12)°/89.4(5)°, and

164   92.7(12)°/91.6(1)° for E = O, S, Se, and Te, respectively (M=Eu/M=Am), which are

165 consistent between the Eu and Am complexes within the standard deviations of the

166 average values. These results indicate that the coordination sphere, symmetry, and

167 geometry are uniformly comparable between the chalcogens in the case of the

168 HN(EPR$_2$)$_2$ ligands.

169   *Complexation energy*

170 The ΔG values for the complexation reaction were estimated using Eqs. 2-5 and are

171 summarized in Table 2. It was found that the ΔG values decreased in the order of E = O,

172 S, Se, and Te for both Eu and Am systems. This tendency is consistent with the trend in

173 the stability of complexes of chalcogen-donor ligands with hard acid ions and indicates

174 that the stability of complexes of Eu(III) and Am(III) ions with chalcogen-donor ligands

175 relative to that of the corresponding hydrated species follows the hard acid classification

176 [4]. This tendency is dominated by variations in ΔE^{tot} values, because ΔG^{corr} values are

177 not so sensitive to the chalcogen-donor ligands. When comparing ΔE^{tot} values between

178 Eu and Am systems, the Eu complex is more stable than the Am complex in the case of

179 the E = O system, whereas the Am complex is more stable than the Eu complex in the

180 case of the E = S system. The reverse trends in stability for Eu(III) and Am(III) ions with

181 O- and S-donor ligands are consistent with experimental and computational results for the

182 Am/Eu selectivity of HO$_2$PR$_2$ and HS$_2$PR$_2$ ligands [3, 12, 13]. This indicates that the

183 Am/Eu selectivity is strongly dependent on differences in not the coordination

184 environment but the donor atoms, because the [M{N(EPMe$_2$)$_2$}$_3$] complexes have the

185 same coordination symmetry irrespective of the chalcogen-donor ligands. We also found

186 that the selectivity for Am over Eu of the chalcogen-donor ligands follows the order O $\ll$

187 S $\approx$ Se $\geq$ Te, although this selectivity has never been investigated experimentally. This

188 tendency is consistent with the trend in the stability of complexes of chalcogen-donor

189 ligands with soft acid ions and indicates that the relative stability of Am-chalcogen

190 complexes with respect to the corresponding Am-H$_2$O complexes, when compared with

191 that of Eu-complexes, follows the soft acid classification [4]. These results suggest that

192 Eu(III) and Am(III) ions display hard acid character with chalcogen-donor ligands, as it

193 was observed in the *Geometry optimization* section that the nature of the bonding

194   between the metal ions and the chalcogen-donor atoms was ionic. This indicates that the

195   soft acid character of Am(III) ions was revealed for the first time when the relative

196   stabilities of the metal-chalcogen and hydrated complexes were compared between Eu

197   and Am systems.

198   *Population analysis*

199   Table 3 shows the Mulliken atomic spin populations (ρ_{spin}) of the metal ion in the

200   [M{N(EPMe$_2$)$_2$}$_3$] complexes, which is a useful indicator of covalent interactions in

201   metal complexes [28]. A comparison of the ρ_{spin} values between the Eu and Am

202   complexes indicates that the ρ_{spin} value of an Am complex is larger than that of the

203   corresponding Eu complex, except for the E = O complexes. This tendency is

204   qualitatively correlated with the Am(III)/Eu(III) selectivity; in other words, S-, Se-, and

205   Te-donor ligands selectively coordinate to Am(III) ions in comparison with Eu(III) ions,

206   whereas O-donor ligands preferentially coordinate to Eu(III) ions in comparison with

207   Am(III) ions. The d- and f-orbital electrons were found to make the dominant

208   contribution to the ρ_{spin} value for all the complexes. Figures 3 and 4 show selected

209   illustrations of the MOs of the complexes[M{N(EPMe$_2$)$_2$}$_3$] (M = Eu, Am; E = O, S). On

210   comparing the shapes of the MO surfaces, the MOs that include contributions from the

211   valence d-orbitals of the metal atom have similar shapes and almost the same bonding

212   overlaps between the metal atom and the donor atoms as *bonding-type* orbitals, as the

213   orbitals overlap in coordinate phases independently of the metal atom and the chalcogen-

214   donor atoms (Figure 3). However the MOs that include contributions from the valence f-

215   orbitals of the metal atom have significantly different shapes and overlaps between the

216   metal atom and the donor atoms (Figure 4). The f-type MOs exhibit either no or weak

217   overlapping in the cases of the Eu complexes. On the other hand, the f-orbitals of Am

218   atoms strongly overlap the orbitals of O-donor atoms in the form of *antibonding-type*

219   orbitals, which overlap in opposite phases, but with S-donor atoms they form *bonding-*

220   *type* orbitals.

221   In order to investigate the type of bonding between the metal atom and the donor atoms,

222   we performed MOOP analysis using our previous method [12, 13]. We show curves of

223   the partial density of states (PDOS) of the metal atom together with the MOOP between

224   the d-orbitals (Figure 5) or f-orbitals (Figure 6) of the metal atom and the chalcogen-

225   donor atoms for [M{N(EPMe$_2$)$_2$}$_3$]. On comparing the MOOP curves for Eu and Am

226   systems shown in Figure 5, the MOOP is distributed at almost the same orbital energies

227   and also has the same positive values in all regions irrespective of the chalcogen-donor

228   ligands. This indicates that the d-orbitals of the metal atom overlap the orbitals of the

229   chalcogen-donor atoms in the form of *bonding-type* orbitals independently of the metal

230   atoms or the chalcogen-donor atoms. On comparing the MOOP distributions shown in

231   Figure 6, the distributions are significantly different between the Eu and Am systems. We

232   focus on the MOOP distribution in the region in which PDOS is mainly distributed. In the

233   case of the Eu complexes, the MOOP is not distributed in the region from −20 to −10 eV

234   except for the E = O system, which has a positive distribution in this region. In the case

235   of the Am complexes, the MOOP is distributed in the region from −15 to −5 eV with a

236   positive sign except for the E = O system, which has a strong negative distribution in this

237   region. These results indicate that the S, Se, and Te-donor atoms have *bonding-type*

238   overlaps with the f-orbitals of Am atoms but do not overlap those of Eu atoms, whereas

239   the O-donor atoms have *antibonding-type* overlaps with the f-orbitals of Am atoms but

240   *bonding-type* overlaps with those of Eu atoms. This tendency in the MOOP between the

241   f-orbitals of the metal atoms and the chalcogen-donor atoms is correlated with the

242   Am(III)/Eu(III) selectivity of the chalcogen-donor ligands. The *bonding-type* interaction

243   between the f-orbitals of Am atoms and the ligands in which E = S, Se, and Te leads to

244   relatively high stability in Am complexes in comparison with Eu complexes. However

245   the ligand in which E = O has *bonding-type* interactions with the f-orbitals of Eu atom

246   and *antibonding-type* interactions with those of Am atoms, which leads to high selectivity

247   for Eu(III) ions over Am(III) ions. Our conclusion that the bonding contribution of the f-

248   orbitals, but not the d-orbitals, of the metal atoms is correlated with the Am(III)/Eu(III)

249   selectivity suggests that evidence of the hardness or softness of f-block metal ions can be

250   based on the covalency of bonding in f-block complexes. This work is expected to

251   contribute to systematic discussions of covalency in f-block metal atoms by incorporating

252   Pearson's HSAB rule as well as the molecular design of novel extraction reagents for

253   separating MA ions from Ln ions.

254   **Conclusions**

255   DFT calculations were applied to the Am(III)/Eu(III) selectivity of chalcogen-donor

256   ligands using model complexes of the formula [M{N(EPMe$_2$)$_2$}$_3$] that possess the same

257   coordination geometry in order to extend the discussion of chemical bonding in f-block

258   complexes. The equilibrium structures have the same symmetry irrespective of the metal

259   atom or chalcogen-donor ligand. The Am(III)/Eu(III) selectivity based on the

260   complexation reaction indicated that the ligands in which E = S, Se, and Te selectively

261   coordinate to Am(III) ions, but the ligand in which E = O selectively coordinates to

262   Eu(III) ions. Analysis of the MOOP between the metal atom and the chalcogen-donor

263   atoms suggested that the ligand in which E = S, Se, and Te have bonding-type

264   interactions with the f-orbitals of Am atoms, but the ligand in which E = O has

265   antibonding-type interactions with the f-orbitals of Am atoms. This result indicated that

266   the contribution of the f-orbitals of Am atoms to bonding with chalcogen-donor atoms is

267   a source of Am(III)/Eu(III) selectivity. The tendency of Am(III)/Eu(III) selectivity is also

268   consistent with the trend in the stability of complexes, which follows the soft acid

269   classification by HSAB rule. We believe that the present work will lead to the

270   development of quantitative discussions of covalency of in metals and ligands by

271   incorporating the HSAB rule. Furthermore, an extension of this study to pnictogen-donor

272   ligands is now under way.

275   **References**

276   1. Oigawa H, Nishihara K, Nakayama S, Morita Y (2010) Concept of waste management

277   and geological disposal incorporating partitioning and transmutation technology.

278   Proceedings of 10th Information Exchange Meeting 123-131

279   2. Nash KL (1993) A review of the basic chemistry and recent developments in trivalent

280   f-elements separations. Solvent Extr Ion Exch 11:729-768

281   3. Jensen MP, Bond AH (2002) Influence of aggregation on the extraction of trivalent

282   lanthanide and actinide cations by Cyanex 272, Cyanex 301, and Cyanex 302. Radiochim

283   Acta 90:205-209

284   4. Pearson RG (1963) Hard and Soft Acids and Bases. J Am Chem Soc 85:3533-3539

285   5. Nagame Y, Hirata M, Nakahara H (2011) In: Vértes A, Nagy S, Klencsár Z, Lovas RG,

286   Rösch F (ed) Handbook of Nuclear Chemistry Springer, Berlin, Heidelberg

287   6. Kaltsoyannis N (2003) Recent development in computational actinide chemistry.

288   Chem Soc Rev 32:9-16

289   7. Schreckenbach G, Shamov GA (2010) Theoretical actinide molecular science. Acc

290   Chem Res 43:19-29

291   8. Platas-Iglesias C, Roca-Sabio A, Regueiro-Figueroa M, Esteban-Gómez D, de Blas A,

292   Rodrígues-Blas T (2011) Curr Inorg Chem 1:91-116

293   9. Wang D, van Gunsteren WF, Chai Z (2012) Recent advances in computational actinoid

294   chemistry. Chem Soc Rev 41:5836-5865

295   10. Cao X, Heidelberg D, Ciupka J, Dolg M (2010) First-principles study of the

296   separation of Am^{III}/Cm^{III} from Eu^{III} with Cyanex301. Inorg Chem 49:10307-10315

297   11. Cao X, Zhang J, Weissmann D, Dolg M, Chen X (2015) Accurate quantum chemical

298   modeling of the separation of Eu^{3+} from Am^{3+}/Cm^{3+} by liquid-liquid extraction with

299   Cyanex272. Phys Chem Chem Phys 17:20605-20616

300 12. Kaneko M, Miyashita S, Nakashima S (2015) Bonding study on the chemical
301 separation of Am(III) from Eu(III) by S-, N-, and O-donor ligands by means of all-
302 electron ZORA-DFT calculation. Inorg Chem 54:7103-7109

303 13. Kaneko M, Watanabe M, Miyashita S, Nakashima S (2017) Roles of d- and f-orbital
304 electrons in the complexation of Eu(III) and Am(III) ions with alkyldithiophosphinic acid
305 and alkylphosphinic acid using scalar-relativistic DFT calculations. J Nucl Radiochem
306 Sci 17:9-15

307 14. Gaunt AJ, Reilly SD, Enriquez AE, Scott BL, Ibers JA, Skar P, Ingram KIM,
308 Kaltsoyannis N, Neu MP (2008) Experimental and theoretical comparison of actinide and
309 lanthanide bonding in M[N(EPR$_2$)$_2$]$_3$ complexes (M = U, Pu, La, Ce; E = S, Se, Te; R =
310 Ph, *i*Pr, H). Inorg Chem 47:29-41

311 15. Pietraszkiewicz M, Pietraszkiewicz O, Karpiuk J, Karpiuk E, Borowiak T,
312 Dutkiewicz (2012) The first ternary europium tetraphenylimidodiphosphinate complex:
313 X-ray structure and photoluminescent properties. Inorg Chim Acta 387:426-430

314 16. Burns JH, Danford MD (1969) The crystal structure of cesium
315 tetrakis(hexafluoroacetylacetonato)europate and -americate. Isomorphism with the
316 Yttrate. Inorg Chem 8:1780-1784

317 17. Burns JH, Baldwin WH (1977) Crystal structures of aquotris(salicylato)samarium(III)
318 and aquotris(salicylato)americium(III). Inorg Chem 16:289-294

319 18. Tian G, Shuh AK, Beavers CM, Teat SJ (2015) A structural and spectrophotometric
320 study on the complexation of Am(III) with TMOGA in comparison with the extracted
321 complex of DMDOOGA. Dalton Trans 44:18469-18474

322 19. Kaneko M, Watanabe M, Matsumura T (2016) The separation mechanism of Am(III)
323 from Eu(III) by diglycolamide and nitrilotriacetamide extraction reagents using DFT
324 calculations. Dalton Trans 45:17530-17537

325   20. Ribeiro RF, Marenich AV, Cramer CJ, Truhler DG (2011) Use of solution-phase

326   vibrational frequencies in continuum models for the free energy of solvation. J Phys

327   Chem B 115:14556-14562

328   21. McCann BW, de Silva N, Windus TL, Gordon MS, Moyer BA, Bryantsev VS, Hay

329   BP (2016) Computer-aided molecular design of bisphosphine oxide lanthanide

330   extractants. Inorg Chem 55:5787-5803

331   22. Neese F (2012) The ORCA program system. WIREs Comput Mol Sci 2:73-78

332   23. van Lenthe E, Snijders JG (1993) Relativistic regular two-component Hamiltonians. J

333   Chem Phys 99:4597-4610

334   24. van Wüllen C (1998) Molecular density functional calculations in the regular

335   relativistic approximation: Method, application to coinage metal diatomics, hydrides,

336   fluorides and chlorides, and comparison with first-order relativistic calculations. J Chem

337   Phys 109:392-399

338   25. Becke AD (1988) Density-functional exchange-energy approximation with correct

339   asymptotic behavior. Phys Rev A 38:3098-3100

340   26. Perdew JP (1986) Density-functional approximation for the correlation energy of the

341   inhomogeneous electron gas. Phys Rev B 33:8822-8824

342   27. Grimme S (2006) Semiempirical hybrid density functional with perturbative second-

343   order correlation. J Chem Phys 124:034108_1-034108_16

344   28. Kaneko M, Miyashita S, Nakashima S (2015) Benchmark study of the Mössbauer

345   isomer shifts of Eu and Np complexes by relativistic DFT calculations for understanding

346   the bonding nature of f-block compounds. Dalton Trans 44:8080-8088

347   29. Pantazis DA, Chen X-Y, Landis CR, Neese F (2008) All-electron scalar relativistic

348   basis sets for third-row transition metal atoms. J Chem Theory Comput 4:908-919

349   30. Pantazis DA, Neese F (2009) All-electron scalar relativistic basis sets for the
350   lanthanides. J Chem Theory Comput 5:2229-2238

351   31. Pantazis DA, Neese F (2011) All-electron scalar relativistic basis sets for the
352   actinides. J Chem Theory Comput 7:677-684

353   32. Wiebke J, Cao X, Dolg M (2007) Approaching actinide(+III) hydration from first
354   principles. Phys Chem Chem Phys 9:459-465

355   33. Ciupka J, Cao X, Wiebke J, Dolg M (2010) Computational study of lanthanide(III)
356   hydration. Phys Chem Chem Phys 12:13215-13223

357   34. Neese F (2003) An improvement of the resolution of the identity approximation for
358   the formation of the Coulomb matrix. J Comput Chem 24:1740-1747

359   35. Neese F, Wennmohs F, Hansen A, Becker U (2009) Efficient, approximate and
360   parallel Hartree-Fock and hybrid DFT calculations. A 'chain-of-spheres' algorithm for
361   the Hartree-Fock exchange. Chem Phys 356:98-109

362   36. Momma K, Izumi F (2008) VESTA: a three-dimensional visualization system for
363   electronic and structural analysis. J App Cryst 41:653-658

364   37. Mulliken RS (1955) Electronic population analysis on LCAO-MO molecular wave
365   functions. I. J Chem Phys 23:1833-1840

366   38. Mulliken RS (1955) Electronic population analysis on LCAO-MO molecular wave
367   functions. III. Effects of hybridization on overlap and gross AO populations. J Chem
368   Phys 23:2338-2342

369   39. Ingram KIM, Tassell MJ, Gaunt AJ, Kaltsoyannis N (2008) Covalency in the f
370   element-chalcogen bond. Computational studies of $M[N(EPR_2)_2]_3$ (M = La, Ce, Pr, Pm,
371   Eu, U, Np, Pu, Am, Cm; E = O, S, Se, Te; R = H, ^{i}Pr, Ph). Inorg Chem 47:7824-7833

372   40. Shannon RD (1976) Revised effective ionic radii and systematic studies of
373   interactomic distances in halides and chalcogenides. Acta Cryst A32:751-767

374 **Table 1** Metal-chalcogen distances of the complexes [M{N(EPR$_2$)$_2$}$_3$] (Å)

Complexes		Calculated		Experimental	$r^{ion}(M^{3+}) + r^{ion}(E^{2-})$
		This work	Ref. 39		[40]
E=O	M=Eu	2.321(11)	2.335	2.302 (M=Eu)	2.35
	M=Am	2.358(10)	2.358	-	2.38
E=S	M=Eu	2.849(8)	2.873	2.892 (M=La)	2.79
	M=Am	2.831(7)	2.835	2.819 (M=Pu)	2.82
E=Se	M=Eu	2.971(17)	2.985	3.019 (M=La)	2.93
	M=Am	2.952(3)	2.940	2.917 (M=Pu)	2.96
E=Te	M=Eu	3.176(19)	3.20	3.224 (M=La)	3.16
	M=Am	3.144(4)	3.13	3.123 (M=Pu)	3.19

375

376

377   **Table 2** Calculated energies in complexation reaction in Eq. 1 (kJ mol^{-1})

Reaction	$\Delta G(M)$		$\Delta G(Am) - \Delta G(Eu)$	$\Delta E^{tot}(Am) - \Delta E^{tot}(Eu)$
	M=Eu	M=Am		
E=O	−508.2	−497.3	−10.8	−7.7
E=S	−266.8	−296.2	29.3	34.3
E=Se	−218.8	−249.3	30.5	34.6
E=Te	−199.2	−227.6	28.4	31.4

378

379

380   **Table 3** Mulliken spin population (ρ_{spin}) values of the complexes $[M\{N(EPMe_2)_2\}_3]$

381   (electrons)

Complexes		ρ_{spin}				
		all	s	p	d	f
E=O	M=Eu	6.036	0.006	0.011	0.035	5.984
	M=Am	6.020	0.010	0.007	0.051	5.952
E=S	M=Eu	6.113	0.014	0.025	0.085	5.989
	M=Am	6.120	0.022	0.031	0.110	5.956
E=Se	M=Eu	6.135	0.017	0.028	0.099	5.990
	M=Am	6.154	0.027	0.038	0.132	5.957
E=Te	M=Eu	6.169	0.019	0.033	0.126	5.991
	M=Am	6.208	0.032	0.050	0.173	5.953

382

383

(a) HO₂PR₂   **(b) HS₂PR₂**   **(c) HN(EPR₂)₂**
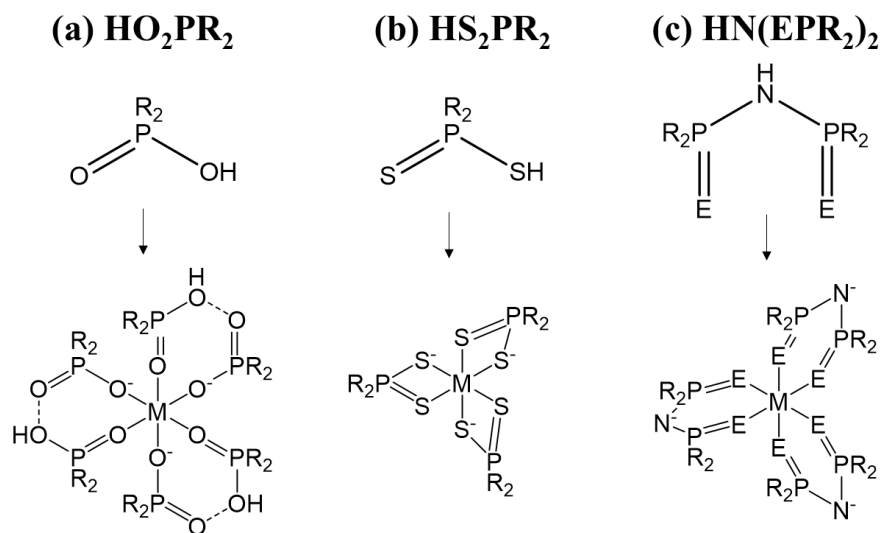
384

385   **Fig. 1** Chemical structural formulas of chalcogen-donor ligands for (a) HO_2PR_2, (b)

386   HS_2PR_2, and (c) $HN(EPR_2)_2$ and their complexes

387

388
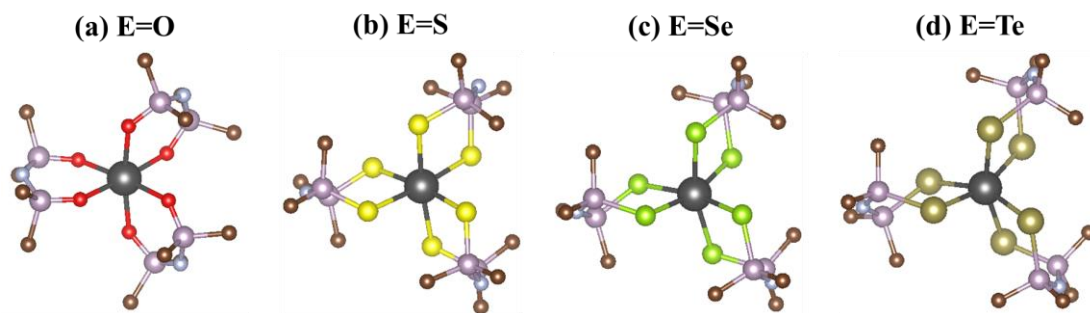
Fig. 2 Three-dimensional descriptions of the complexes [M{N(EPMe$_2$)$_2$}$_3$] (E = (a) O, (b) S, (c) Se, and (d) Te) in which black, red, yellow, green, deep green, purple, blue, and brown spheres show metal, oxygen, sulfur, selenium, tellurium, phosphorus, nitrogen, and carbon atoms, respectively, and hydrogen atoms are omitted for clarity

(a) E = O **(b) E = S**

M = Eu

M = Am

396
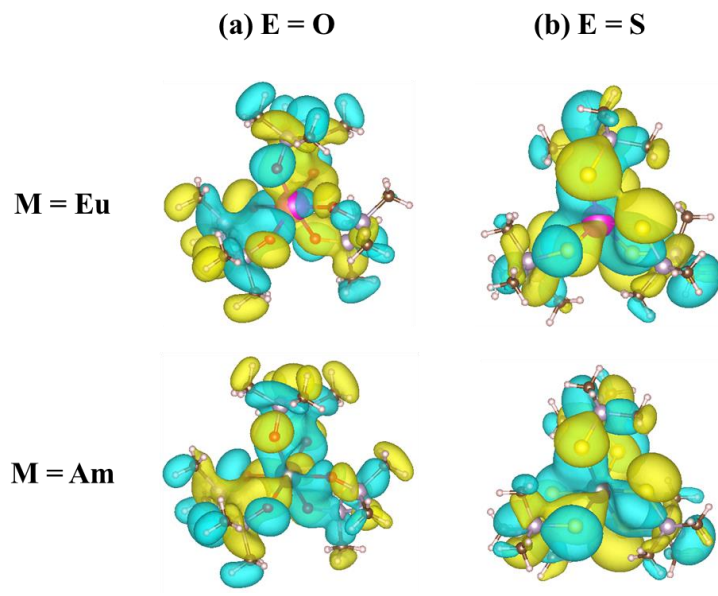
Fig. 3 Selected d-type MO surfaces of the complexes [M{N(EPMe$_2$)$_2$}$_3$] (E = (a) O and
(b) S)

399

(a) E = O   **(b) E = S**

M = Eu

M = Am
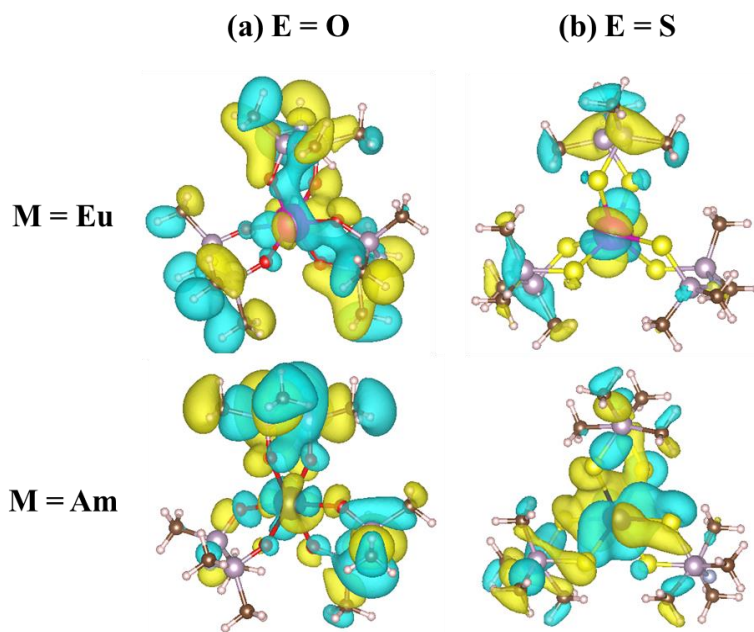
400

401   **Fig. 4** Selected f-type MO surfaces of the complexes [M{N(EPMe$_2$)$_2$}$_3$] (E = (a) O and
402   (b) S)

403

404
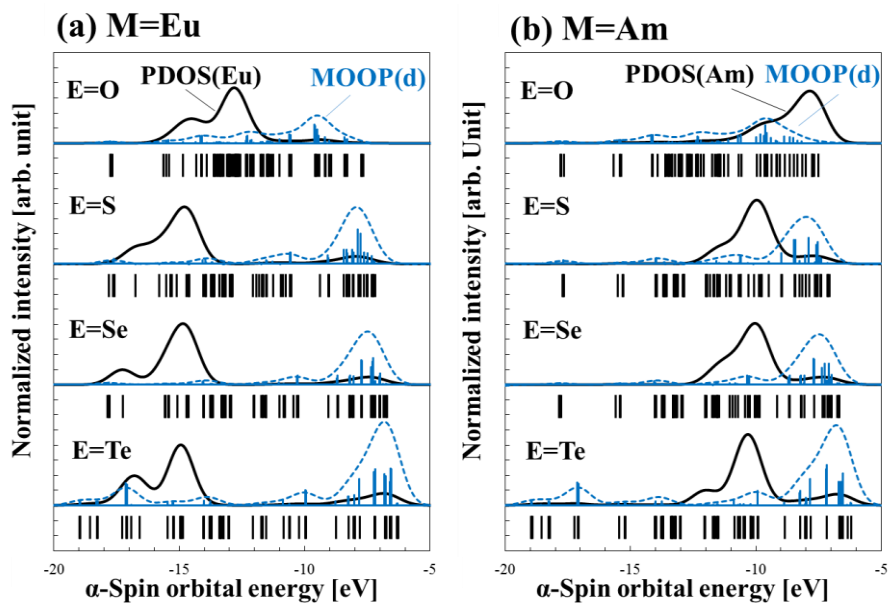
Fig. 5 Curves of the partial density of states (PDOS) of the metal atom together with the MOOP between the d-orbitals of the metal atom and the chalcogen-donor atoms for $[M\{N(EPMe_2)_2\}_3]$ (M = (a) Eu and (b) Am), which were convoluted with a half-width value of 0.5 eV
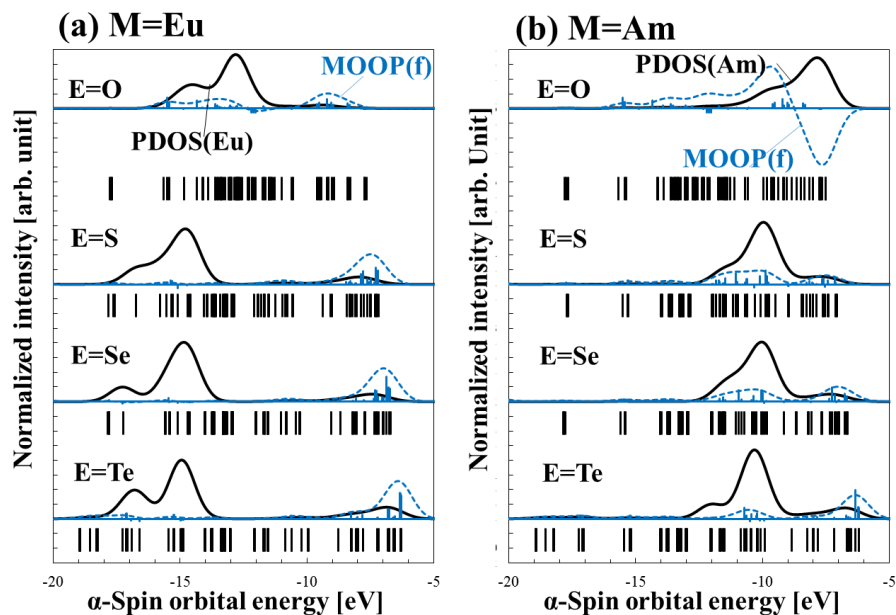
Fig. 6 Curves of the partial density of states (PDOS) of the metal atom together with the MOOP between the f-orbitals of the metal atom and the chalcogen-donor atoms for [M{N(EPMe$_2$)$_2$}$_3$] (M = (a) Eu and (b) Am), which were convoluted with a half-width value of 0.5 eV